Journal of Power Sources 196 (2011) 8188–8196

Contents lists available at ScienceDirect

Journal of Power Sources

journal homepage: www.elsevier.com/locate/jpowsour

Novel mesoporous carbon ceramics composites as electrodes for direct methanol fuel cell

Jean Marcel R. Gallo [a,b], Giorgio Gatti [b], Alessandro Graizzaro [c], Leonardo Marchese [b,**], Heloise O. Pastore [a,*]

[a] Grupo de Peneiras Moleculares Micro e Mesoporosas, Instituto de Química, UNICAMP, CP 6154, CEP 13083-970, Campinas, SP, Brazil
[b] Dipartimento di Scienze e Tecnologie Avanzate and Centro Interdisciplinare Nano-SiSTeMI, Università del Piemonte Orientale "A. Avogadro", Viale T. Michel 11, I-15121 Alessandria, Italy
[c] HySyLab, Environment Park, Via Livorno 60, 10144 Torino, Italy

ARTICLE INFO

Article history:
Received 28 February 2011
Received in revised form 3 May 2011
Accepted 6 May 2011
Available online 17 May 2011

Keywords:
Mesoporous carbon ceramic
Mesoporous molecular sieve
Direct methanol fuel cell

ABSTRACT

In this work, a new family of materials for electrodes of direct methanol fuel cell (DMFC) is presented. Mesoporous carbon ceramics (MCCs) are obtained by the addition of commercial graphite into the synthesis gel of SBA-15 mesoporous silica with SiO_2/C weight ratios of 1/1 and 1/3. X-ray diffraction confirms both the formation of organized silica and the presence of graphite, and nitrogen physisorption measurements show that the presence of a graphitic phase does not interfere in the silica pore diameter although it diminishes the surface area. The MCCs modified with Pt or PtRu are tested as DMFC electrodes and compared with the commercial support Vulcan XC-72R. When used as cathode, the system using MCC-SBA-15 with SiO_2/C weight ratios of 1/1 presents a negligible performance, while the MCC-SBA-15 with SiO_2/C weight ratios of 1/3 is 2.9 times less active than the commercial support. On the other side, when used as anode, the MCC-SBA-15 with SiO_2/C weight ratios of 1/3 displays performances comparable to Vulcan XC-72R.

1. Introduction

Direct methanol fuel cell (DMFC) is today the third (after PEMFC and SOFC) most researched fuel cell technology in industry [1]. Compared with the other types, its advantages are the possibility of size reduction and of using liquid combustible instead of gaseous ones. Although the DMFC is considered near to the commercial application [2], many efforts have been spent in developing new polymeric membranes, which ideally could diminish the methanol crossover; and new metal alloy catalysts, to improve the anodic reaction rate and yield.

Besides the catalytically active metal or alloy, the DMFC electrodes contain two more phases: (i) a proton conductive polymer, to decrease the interface resistance between electrode and electrolyte and; (ii) an electrical conductive support, responsible for the electron conductivity from the metal site to the electrical circuit [3]. Furthermore, the support, classically carbon, is not a mere inert material: in a carbon-supported metal–catalyst system, for example, it alters the system Galvani potential, raises the electronic density in the catalysts, and lowers the Fermi level, accelerating, then, the electrode processes [4].

For PEMFC and DMFC, metal particles are commonly supported on Carbon Black, such as Acetylene Black, Vulcan XC-72, Ketjen Black, etc., which are usually manufactured by pyrolysis of hydrocarbons such as natural gas or oil fractions taken from petroleum processing [5]. Due to its low Ohmic resistance and high specific surface area (ca. 250 $m^2\ g^{-1}$), Vulcan XC-72 is the most used metal support on DMFC and PEMFC commercial catalysts [5]. Alternative supports with surface area higher than Vulcan XC-72R, such as nanostructured and mesoporous carbon have been proposed for DMFC and showed interesting results [5].

The research for new supports is not as intensive as the one for membranes or metal alloys, but in recent years, a series of new nanostructured carbon materials were explored as catalyst supports. Carbon nanotubes (CNTs) are the most studied nanostructured carbons, and have shown promising results as catalyst support for PEMFC and DMFC [5]. CNT-supported Pt catalyst with 12 wt.% Pt loading as PEMFC anode presented a 10% higher voltage, and twice the power density than that of Carbon Black supported with 29 wt.% Pt loading [6]. Pt supported on multi-walled carbon nanotube (MWNT) was studied as an electrode for methanol oxidation and showed a mass activity at 0.7 V (vs. DHE) of 14.7 mA mg^{-1} against 2.2 mA mg^{-1} for Pt/Vulcan XC-72 [7]. Other experiments show Pt/MWNT ca. 20 times more active than the

* Corresponding author. Tel.: +55 19 35213095; fax: +55 19 35213023.
** Corresponding author. Tel.: +39 0131 360262; fax: +39 0131 360250.
E-mail addresses: leonardo.marchese@mfn.unipmn.it (L. Marchese), gpmmm@iqm.unicamp.br (H.O. Pastore).

0378-7753
doi:10.1016/j.jpowsour.2011.05.008

bulk Pt electrode [8]. Pt supported on single-wall carbon nanotube (SWNT) has also exhibited higher catalytic activity as DMFC cathode and anode if compared to an unsupported Pt electrode [9].

Although carbon nanotubes have shown promising results as catalyst supports for DMFCs, their syntheses still face some challenges, especially the ones linked to their high cost and to the lack of adequate large scale preparation [5].

Mesoporous carbons are also promising catalyst support for DMFC anode catalysis [5]. Yu et al. [10] studied a series of PtRu supported on porous carbons with pore diameters between 10 and 1000 nm and found that the material with pore size of 25 nm reaches a performance 43% higher than that of the commercially available PtRu/C catalyst. Spherical carbon capsules with a hollow core and mesoporous shell structures (HCMS) and microporous active carbon microspheres have also shown to be better supports than Vulcan XC-72 [11,12].

The research for new metal supports for DMFC is limited to carbon materials, since they have high stability in both acidic and basic media and, mainly, good electric conductivity [5].

In 1994, Lev and co-workers [13] published the synthesis of carbon ceramics electrodes (CCE), based on the condensation of sol–gel silica around graphite particles. According to the authors, the composites benefit from the mechanical properties of the silica backbone, from the electron percolation conductivity through the interconnected carbon particles and from the ability to manipulate the silica properties by incorporation of different monomer precursors or sol–gel dopants [14]. The CCE described by Lev had interesting applications, however, the low surface area would limit its use in the fuel cell area. Hence, an alternative would be to make efforts in synthesizing carbon ceramics with high surface area.

In the present work, the synthesis of a high surface area carbon ceramic, the novel mesoporous carbon ceramics (MCCs), is proposed. The applied strategy was to add commercial graphite in the synthesis of the pure silica mesoporous molecular sieve SBA-15. The composites were prepared with a SiO_2/C weight ratio of 1/1 and 1/3. The samples were also modified with Pt or PtRu alloy and tested on DMFC cathode and anode, respectively.

2. Experimental

2.1. Synthesis of SBA-15 mesoporous carbon ceramic (MCC-SBA-15)

The reaction was based on the pure silica SBA-15 original synthesis [15]. In a 250 mL polypropylene beaker, 120.00 g of a 2 mol L^{-1} aqueous HCl solution were added to a solution of 4.00 g of Pluronic P123 (Aldrich) in 30.00 g of water and the solution was stirred for 1 h at 35 °C. Then, 8.50 g of tetraethyl orthosilicate (TEOS, Alfa Aesar) and 2.35 or 7.05 g (for SiO_2/C weight ratio = 1/1 or 1/3, respectively) of graphite (<45 μm, Aldrich) were added and the mixture was stirred for 24 h at the same temperature. The gel was aged for 24 h at 100 °C in an autoclave in static conditions. Finally, the solid was filtered and washed with 4 L of water.

Before the characterization, the organic template, Pluronic P123, was removed from the MCCs by heating the powders from room temperature to 500 °C (1 °C min^{-1}) under nitrogen flow, then, at the same temperature, the gas flow was switched to air and maintained for 5 h. The graphite used for the composite syntheses was analyzed by thermogravimetric analysis (see supporting information, Fig. S1) and showed to burn at temperatures higher than 600 °C under pure oxygen atmosphere.

The MCC-SBA-15 with SiO_2/C weight ratio of 1/1 or 1/3 will be named throughout the text as MCC-SBA-15(1/1) and MCC-SBA-15(1/3), respectively.

2.2. Pt and PtRu deposition

The deposition of 20 wt.% Pt on MCC or Vulcan XC-72R (Cabot) was carried out by stirring 0.30 g of the support in a solution of 384 μmol of chloroplatinic acid hexahydrate ($H_2PtCl_6{\cdot}6H_2O$, Aldrich) in 3 mL of acetone for 1 h. The dispersion was dried for 15 h at 60 °C. For Pt reduction, the powder was heated from room temperature to 300 °C (3 °C min^{-1}) under pure hydrogen flow. This temperature was maintained for 3 h under vacuum [16].

The deposition of 60 wt.% of PtRu alloy was carried out by sonicating 0.050 g of MCC or Vulcan XC-72R in 30 mL of water for 15 min, followed by the addition of a solution containing 2.53 mmol of chloroplatinic acid (H_2PtCl_6, Aldrich), and 2.53 mmol of ruthenium chloride ($RuCl_3$, Aldrich) in 20 mL water. The mixture was stirred for 30 min and then a solution of 400 mg of sodium borohydride (Aldrich) in 50 mL of water was added drop by drop under vigorous stirring. The mixture was stirred for over 2 h, filtered and washed with 500 mL of water [17].

2.3. Characterization techniques

X-ray diffractograms were obtained on a Thermo ARL X-ray diffractometer, operating with CuKα X-ray radiation (X-ray generator current and voltage set at 40 mA and 45 kV).

Nitrogen physisorption measurements were carried out at −196 °C in the relative pressure range from 10^{-6} to 1 P/P_0 using a Quantachrome Autosorb 1MP/TCD instrument. Prior to the analysis the samples were outgassed (residual pressure $p < 10^{-7}$ mbar) at 250 °C for 15 h. Specific surface areas were determined by using Brunauer–Emmett–Teller (BET) equation. Pore size distributions were obtained by applying the non-local density functional theory (NLDFT) method for cylindrical pores using the desorption branch. Microporous surface area and volume were estimated by *t*-plot. The *t*-plot method employs reference curves obtained from a group of data obtained from nonporous adsorbents with surface similar to the material analyzed.

The scanning electron microscopy (SEM) images were done in a Fei Quanta 200 coupled to an energy dispersive spectrometer (EDS) attachment.

Transmission electron microscopy (TEM) images were performed with a JEOL 3010-UHR operating at 300 kV. Samples were dispersed in isopropanol by ultrasound and a drop of the suspension was deposited on a copper grid with a lacey carbon film.

2.4. DMFC tests

Gas diffusion electrodes (GDEs) were prepared by painting the ink (prepared with 30% of excess) in a carbon cloth (GORE) to obtain 2 mg of platinum per square centimeter of GDE (painting method is detailed elsewhere [18]).

The ink for a 6.25 cm^2 cathode was obtained stirring for 2 h 0.0878 g of 20 wt.% Pt on MCC or Vulcan XC-72R (Cabot), 0.367 g of water, 0.367 g of isopropanol and 0.864 g of Nafion (5% solution in water/isopropanol, Aldrich). The ink for the cathode using the commercial Pt(50 wt.%)/Vulcan XC-72R (E-TEK), was prepared using 0.035 g of catalyst, 0.147 g of water, 0.147 g of isopropanol and 0.346 g of Nafion (5% solution in water/isopropanol, Aldrich).

The ink for a 6.25 cm^2 anode was obtained stirring for 2 h 0.0448 g of 60 wt.% PtRu(1:1) on MCC or Vulcan XC-72R (Cabot) or the commercial PtRu(60 wt.%, 1:1)/Vulcan XC-72R (E-TEK), 0.187 g of water, 0.187 g of isopropanol and 0.441 g of Nafion (5% solution in water/isopropanol, Aldrich).

The membrane and electrode assemblies (MEAs) were prepared by hot-pressing two electrodes on both sides of a Nafion® 117 membrane (Aldrich) at 130 °C and 10 bar for 1.5 min.

The DMFC polarization experiments were carried out galvanostatically. The cathode was fed with 300 mL min^{-1} of pure non-humidified air or 100 mL min^{-1} of pure non-humidified oxygen at atmospheric pressure and the anode was fed with 1 mol L^{-1} aqueous methanol solution with 1 mL min^{-1} flow. Further details about the test station used can be found elsewhere [18].

Internal cell resistance was monitored using the fixed frequency impedance meter HIOKI 3560.

3. Results and discussion

3.1. Synthesis and characterization

The syntheses of the MCC were carried out by adding commercial graphite to the mesoporous molecular sieves reaction medium. The graphite was added before the condensation of the silica in order to obtain a more homogeneous dispersion of the silica/graphite mixture. The amount of graphite used in the composite was based on previous works. Lev and co-workers used as the highest SiO_2/C weight ratio 1/3 [19], however, in the present work MCC with SiO_2/C weight ratio of 1/1 was also synthesized.

In order to verify the formation of the SBA-15 structure on the composites, they were characterized by X-ray diffraction (XRD). Due to the hexagonal organization of the mesoporous (P6mm symmetry), the XRD pattern of SBA-15 is expected to present four peaks at $2\theta < 4^\circ$ related to (1 0 0) (most intense), (1 1 0), (2 0 0) and (2 1 0) reflections. If the first peak (1 0 0) appears on $2\theta = X$, the other peaks must appear at ($\sqrt{3}$)X [(1 1 0)], 2X [(2 0 0)] and ($\sqrt{7}$)X [(2 1 0)] [20].

As it can be observed in Fig. 1a, pure silica SBA-15 presents a XRD pattern with all the expected four peaks [15]. The MCC-SBA-15(1/1) (Fig. 1, curve b) and the MCC-SBA-15(1/3) (Fig. 1, curve c) XRD patterns were similar to that of pure silica SBA-15 at $2\theta < 4^\circ$, indicating that the addition of graphite does not interfere in the formation of a well ordered SBA-15 phase on the composites. In the MCCs (Fig. 1, curves b and c), an additional peak at 26.5 2θ due to the (0 0 1) plane of graphite is observed. This result is in agreement with that of Kónya and co-workers [21], who synthesized the mesoporous molecular sieve of silica MCM-41 under acid medium in the presence of graphite and carbon nanotubes and observed that the carbon sources do not influence the mesoporous silica structure formation.

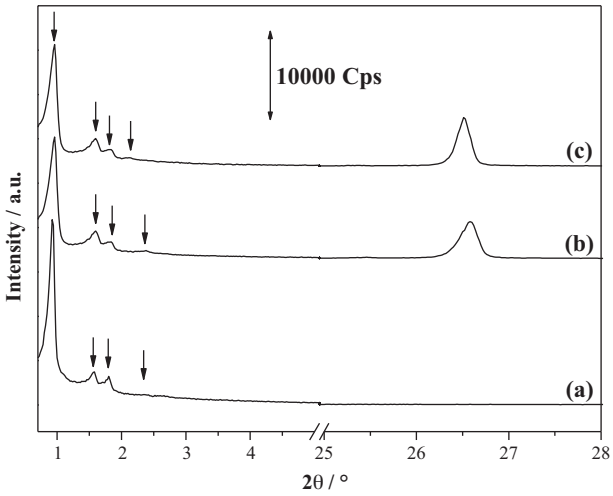

Fig. 1. X-ray patterns of (a) pure silica SBA-15, (b) MCC-SBA-15(1/1) and (c) MCC-SBA-15(1/3).

The influence of the graphite addition on the textural properties (especially in terms of surface area, pore diameters and pore volume) of the mesoporous solids was studied by using nitrogen physisorption at −196 °C. The nitrogen physisorption isotherms obtained for the pure silica SBA-15, MCC-SBA-15(1/1) and MCC-SBA-15(1/3) are shown in Fig. 2A. The obtained data are reported in Table 1.

The pure silica SBA-15 (Fig. 2, curve a) presents a Type IV isotherm, typical for mesoporous molecular sieves [22], in which the adsorption branch is characterized by the formation of the

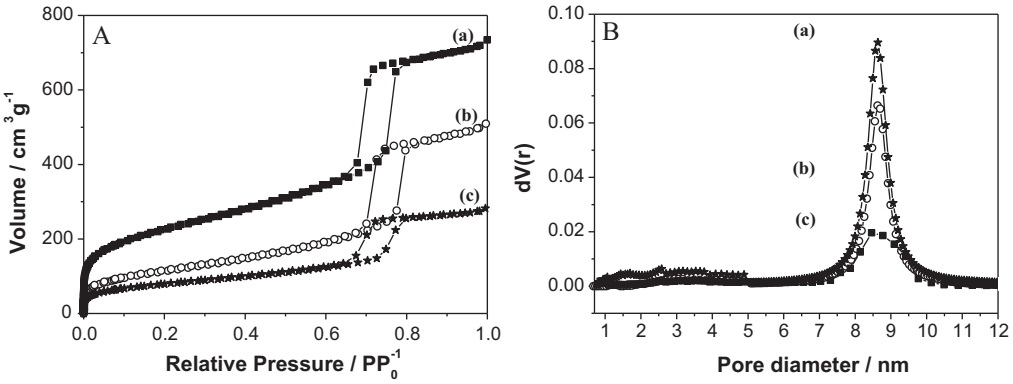

Fig. 2. (A) Isotherms and (B) pore size distribution diagrams of (a) pure silica SBA-15, (b) MCC-SBA-15(1/1) and (c) MCC-SBA-15(1/3).

Table 1
Textural properties of graphite, SBA-15 and MCC-SBA-15.

Sample (SiO_2/C ratio)	S_{BET}[a] ($m^2\ g^{-1}$)	S_M[b] ($m^2\ g^{-1}$)	V_T[c] ($cm^3\ g^{-1}$)	V_M[d] ($cm^3\ g^{-1}$)	D_p[e] (nm)
Graphite	4	–	0.006	–	–
SBA-15	805	179	1.08	0.08	8.6
MCC-SBA-15(1/1)	412	18	0.54	0.003	8.6
MCC-SBA-15(1/3)	203	–	0.20	–	8.6

[a] Specific surface area.
[b] Microporous area.
[c] Total volume.
[d] Microporous volume.
[e] Mesoporous diameter.

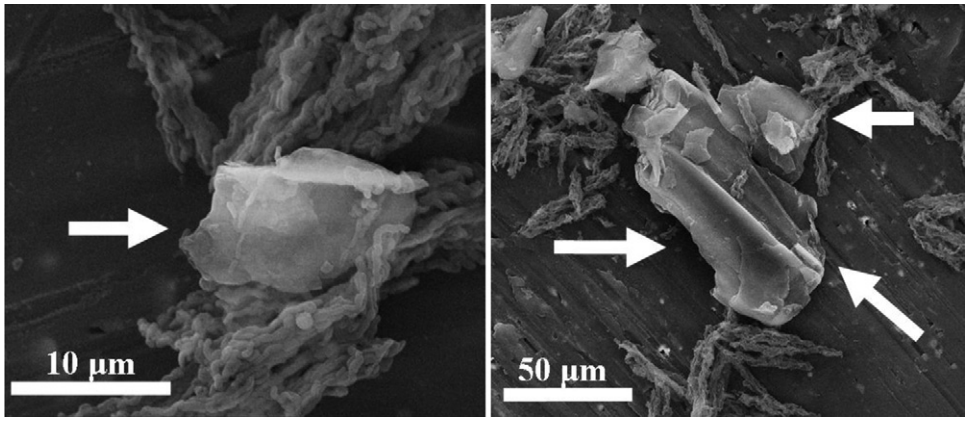

Fig. 3. SEM images of MCC-SBA-15(1/3). Arrows indicate the graphite particle.

nitrogen monolayer and filling of the micropores at $P/P_0 < 0.1$, followed by the capillary condensation on the mesopores at $0.6 < P/P_0 < 0.8$ [22]. The desorption branch is characterized by a H1 hysteresis loop, indicative of well defined cylindrical pores [22]. This kind of hysteresis loop implies in the desorption branch to have the same profile of the adsorption branch, but with the capillary condensation taking place at lower partial pressure.

The MCC-SBA-15(1/1) (Fig. 2A, curve b) and MCC-SBA-15(1/3) (Fig. 2A, curve c) displays isotherms Type IV as pure silica SBA-15 (Fig. 2A, curve a), however, the increase of graphite loading leads to a diminution of adsorbed volumes in both monolayer and capillary condensation steps. The graphite isotherm (see supporting information, Fig. S2) reveals a surface area of 4 $m^2\ g^{-1}$ and a total pore volume of 0.006 $cm^3\ g^{-1}$ while SBA-15 presents a surface area of 806 $m^2\ g^{-1}$ and a total pore volume of 1.08 $cm^3\ g^{-1}$ (Table 1). Since the surface area and total pore volume are obtained as a function of the weight, the increase of a low surface area phase (graphite) in the composites will, naturally, lead to a decrease of the overall (graphite + SBA-15) surface area and total pore volumes. Thus, it is expected that the MCC-SBA-15(1/1), composed of 50% SBA-15 and 50% of graphite, should presents approximately half of the pure SBA-15 surface area and total pore volumes and the MCC-SBA-15(1/3), composed of 25% SBA-15 and 75% of graphite, would present approximately one fourth. These previsions are in fact confirmed, as shown in Table 1.

The microporosity, an intrinsic characteristic of SBA-15, seems to disappear on the composites. However, it is difficult to determine if it was not formed on the composites or if the *t*-plot method cannot identify it. The *t*-plot method is very useful to study well ordered micropores, as those observed on zeolites. For the *t*-plot calculation a group of points from the isotherm must be chosen, and they are easily found on the isotherm of materials with well organized micropores with high surface area. SBA-15 has a broad micropore size distribution (Fig. 2B, curve a) that makes the *t*-plot calculations more complicated and less reliable. In the MCCs composites, that contains 50 or 75 wt.% of graphite, the contribution of the silica phase micropores is very low and, it cannot be found a reliable group of points in their isotherm for the *t*-plot calculation. For this reason, it is difficult to be sure if the decrease on the MCC microporous surface area and volume related to the pure silica SBA-15 can be associated with an influence of the graphite or for a simple limitation of the *t*-plot method.

An interesting observation is that the family of mesopores typically present on SBA-15 (Fig. 2B and Table 1) is not altered by the graphite addition and it is 8.6 for all samples.

In order to understand how silica and graphite are arranged in the composite, the samples were analyzed by SEM. SEM images for MCC-SBA-15(1/1) and MCC-SBA-15(1/3) are similar, thus representative pictures were selected for this work (Fig. 3).

SEM images reveal that MCC-SBA-15 is formed by worm-like particles of approximately 1 μm that form 10–50 μm agglomerates, as usually observed for pure silica SBA-15 [23]. Furthermore, the composite is similar to a mechanical mixture between the graphite (indicated in Fig. 3 by an arrow) and the silica phases. This result may appear trivial since the graphite powder was simply added onto the mesoporous silica synthesis; if the MCC was synthesized with an MCM-41 structure, for example, the silica particles would grow over the graphite (see supporting information, Fig. S3). This happens due to the interaction between the surfactant used for MCM-41 synthesis (cetyltrimethylammonium bromide) and the graphite [24].

From the results in this section, it was shown that the MCC composites present two well defined phases: (i) the graphite, a good electron conductor and (ii) the silica molecular sieve SBA-15, which present organized pores and high surface area. These characteristics make the MCCs potential metal supports for DMFC electrodes.

3.2. MCC-SBA-15 as cathode for DMFC

The first test of the MCCs in DMFC was carried out using the MCC composites as metal supports in the cathode. Hence, 20 wt.%

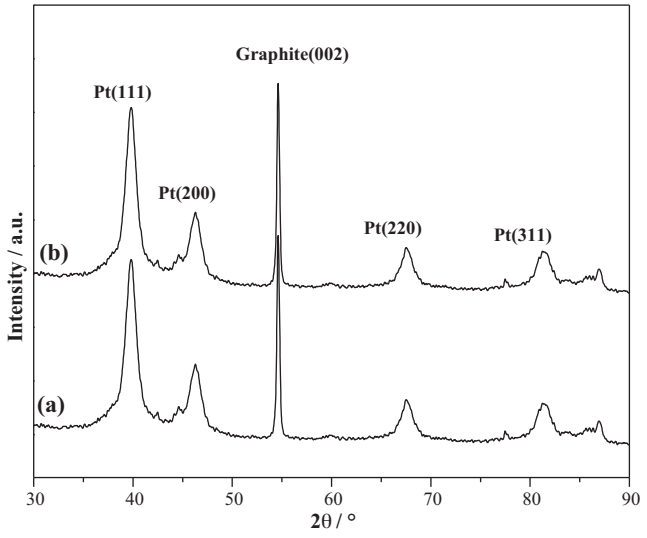

Fig. 4. X-ray pattern of 20 wt.% of platinum supported on (a) MCC-SBA-15(1/1) and (b) MCC-SBA-15(1/3).

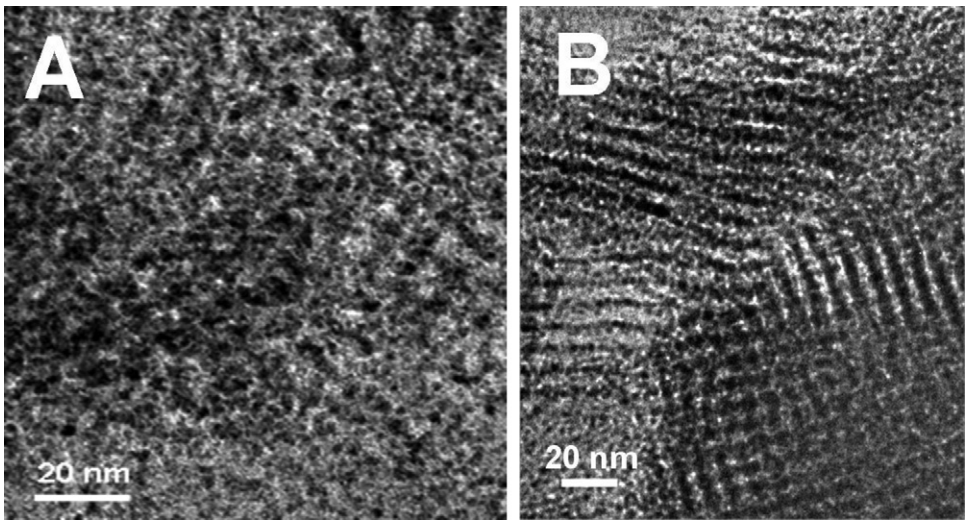

Fig. 5. TEM images of 20 wt.% of platinum supported on (A) MCC-SBA-15(1/1) and (B) MCC-SBA-15(1/3).

of platinum (amount commonly used in literature) was inserted in the MCCs to provide catalytic activity. XRD was used to analyze the Pt/MCC-SBA-15(1/1) (Fig. 4, curve a) and Pt/MCC-SBA-15(1/3) (Fig. 4, curve b).

The XRD patterns of Pt/MCCs are very similar between them and show five diffraction peaks at Bragg angles 39.8°, 46.3°, 67.6°, 81.4° and 86.9° 2θ assigned to (1 1 1), (2 0 0), (2 2 0), (3 1 1) and (2 2 2) planes respectively, of face-centered cubic (Fm3m) platinum crystallites [25]. A further XRD peak at 54.6° 2θ due to the graphite (0 0 2) plane is also observed. The collected XRD data were used to determine the average crystallite size by using the Debye–Scherrer equation (see supporting information) [26]. Although any of the five XRD peaks could be used for the calculation, the (1 1 1) and (2 2 0) peaks are more often used for this purpose. In the cases presented in Fig. 4, the (1 1 1) peak is slightly convoluted with the neighboring peak, thus the (2 2 0) peak was chosen. For both Pt/MCC-SBA-15(1/1) and Pt/MCC-SBA-15(1/3) the platinum average crystallite size was found to be 6.8 nm.

The MCCs were also studied by transmission electron microscopy (TEM), as shown in Fig. 5.

According to the TEM images (Fig. 5), platinum (black dots) is present predominantly in crystallites with dimension between 2 and 3 nm, however, larger particles with dimensions between 10 and 20 nm are also present and this should be the reason of the higher average particle sizes determined by XRD.

The MEA was prepared using the MCC-SBA-15(1/1), MCC-SBA-15(1/3) and the commercial support Vulcan XC-72R modified with 20 wt.% of platinum as cathode. The anode was made with a commercial 60 wt.% PtRu(1:1) on Vulcan XC-72R (E-TEK); and Nafion 117 as electrolyte. The cathode and the anode were fed, respectively, with 300 mL min^{-1} of non-humidified air and 1 mL min^{-1} of a 1 mol L^{-1} aqueous methanol solution. For a first test, the polarization and power curves were obtained at 70 °C as shown in Fig. 6.

For the system using Pt/MCC-SBA-15(1/1) on the cathode, the cell performance reached a maximum of power density of 0.6 mW cm^{-2} and current density of 3.0 mA cm^{-2} at 0.2 V. These values can be considered unsuitable if compared with that of the system using the commercial support, Vulcan XC-72R, on the cathode, which reached values 25 times higher (maximum of power density of 15.4 mW cm^{-2} and current density of 76.4 mA cm^{-2} at 0.2 V). On the other side, the system using Pt/MCC-SBA-15(1/3) on the cathode presented performance only 2.9 times lower than the system using Pt/Vulcan XC-72R. Thus, the MCC-SBA-15(1/1) can be considered as a material not suitable to be used on DMFC electrodes, while MCC-SBA-15(1/3) had promising results. Ambrosio et al. [27] have used the mesoporous carbon Pt/CMK-3 (inverse replica of SBA-15) on the PEMFC cathode at 70 °C and observed that the performance was less than half of that of the system using commercial catalysts. One of the justification gave by the authors was that the Pt/CMK-3 led to a higher internal cell resistance

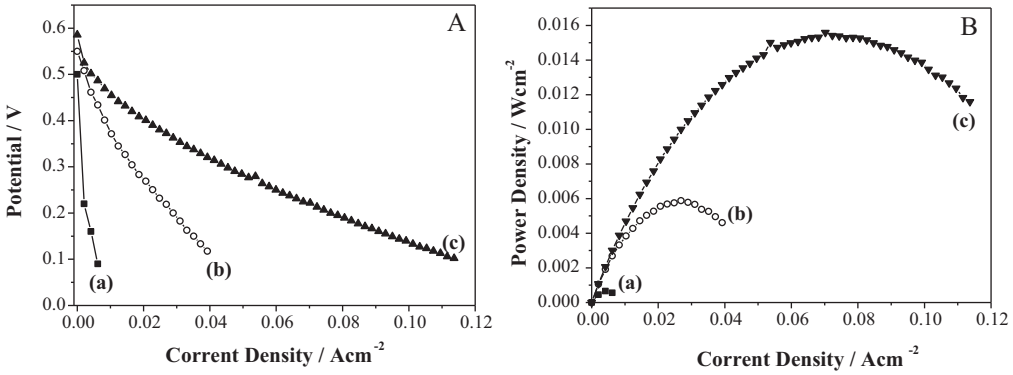

Fig. 6. (A) Polarization curves and (B) power density vs. current density curves for the 20 wt.% Pt supported on (a) MCC-SBA-15(1/1), (b) MCC-SBA-15(1/3) and (c) Vulcan XC-72R as cathode for the DMFC. Anode was assembled with a commercial PtRu/Vulcan XC-72R (E-TEK). Conditions: 70 °C; 300 mL min^{-1} of air; 1 mL min^{-1} of a 1 mol L^{-1} aqueous methanol solution.

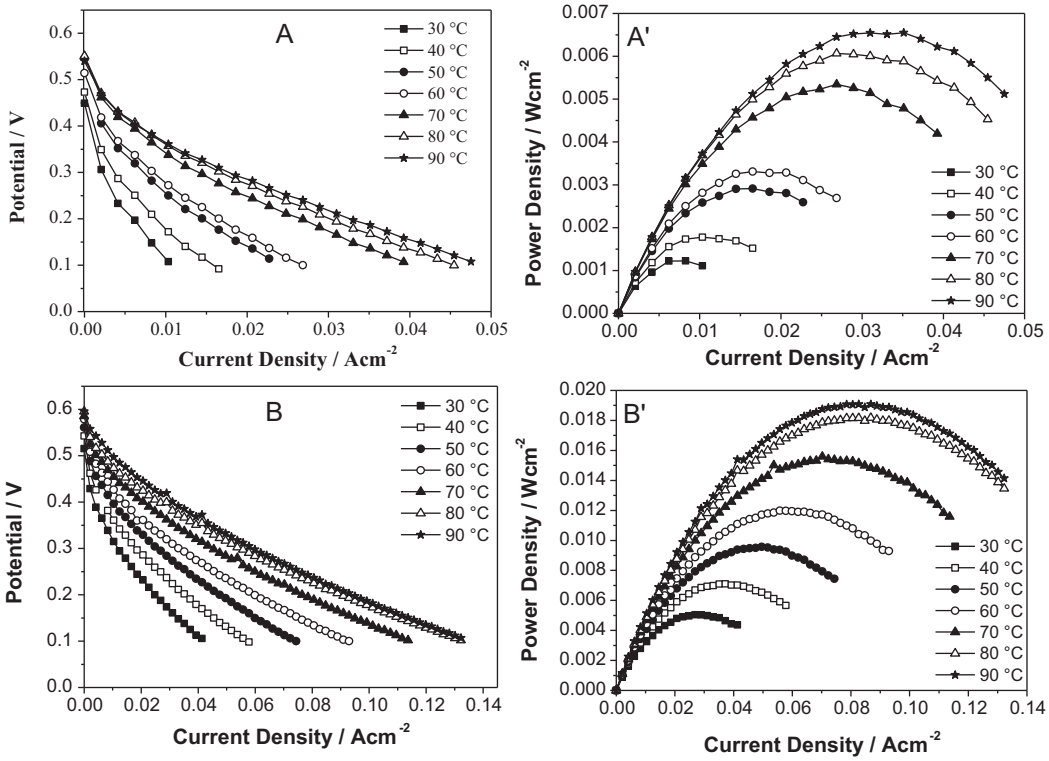

Fig. 7. Polarization and power curves for the DMFC assembled with (A, A′) Pt/MCC-SBA-15(1/3) and (B, B′) Pt/Vulcan XC-72R on the cathode. Anode was prepared using the commercial PtRu/Vulcan XC-72R (E-TEK). Cathode and anode were fed, respectively, with 300 mL min^{-1} of air and 1 mL min^{-1} of a 1 mol L^{-1} aqueous methanol solution.

compared to the commercial catalyst. A similar behavior is observed in the present work. At 70 °C the internal resistance of the cells was 130 Ω for the MCCs-SBA-15(1/3), while for the system using Vulcan XC-72R it was 60 Ω.

Due to the promising results obtained for the Pt/MCC-SBA-15(1/3) on the DMFC cathode at 70 °C, a study varying the temperature from 30 to 90 °C was carried out (Fig. 7A and A′) and the results compared with those obtained for the Pt/Vulcan XC-72R (Fig. 7B and B′).

For both samples it is observed a clear improvement in the cell performance when the temperature is increased. Moreover, the difference between the performances of the system using Pt/MCC-SBA-15(1/3) related to the Pt/Vulcan XC-72R on the cathode diminishes as a function of the temperature, reaching the lowest difference at 70 °C. This behavior could be due to a higher activation temperature of the catalyst when supported on the MCC matrix or due to a problem of water flow in the internal channels of the SBA-15 at low temperatures.

Platinum supported on MCC-SBA-15(1/3) and Vulcan XC-72R was also tested feeding the cathode with pure non-humidified oxygen and the polarization and power curves obtained at 70 °C are shown in Fig. 8. For the cells using MCC-SBA-15(1/3) and Vulcan XC-72R on the cathode the maximum power density were 13.8 and 26.0 mW cm^{-2} and current density at 0.2 V were 68.1 and 128.7 mA cm^{-2}, respectively.

When pure oxygen is used instead of air, the fuel cell can work with a higher power. In this condition, it was observed that the factor of performance difference between the systems using MCC and Vulcan XC-72R on the cathode diminished to 2 (against 2.9, when the cathode was fed with air). The use of the pure oxygen leads to an increase of the reaction rate, as well as the mass transport (of water and proton, on the cathode). Probably the

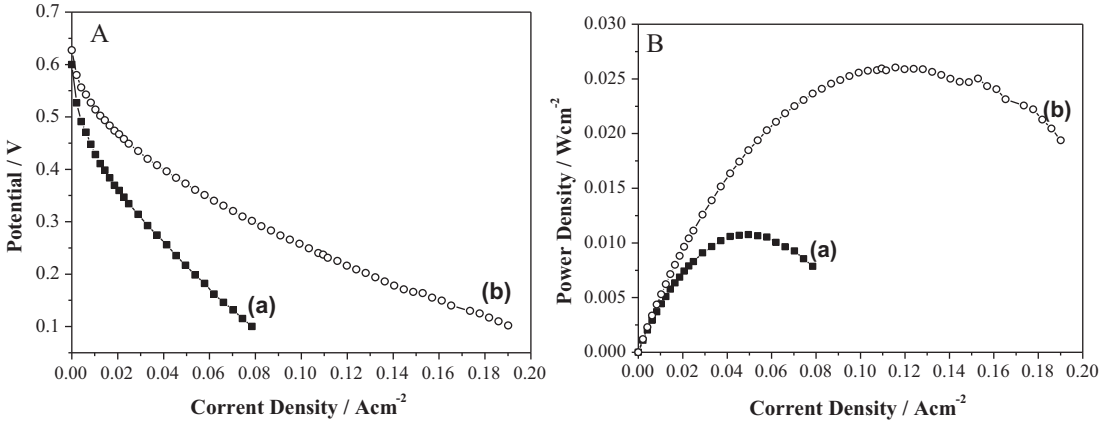

Fig. 8. (A) Polarization curves and (B) power density vs. current density curves for the (a) Pt/MCC-SBA-15(1/3) and the Pt/Vulcan XC-72R as cathode for the DMFC. Conditions: 70 °C; 100 mL min^{-1} of pure oxygen; 1 mL min^{-1} of a 1 mol L^{-1} aqueous methanol solution.

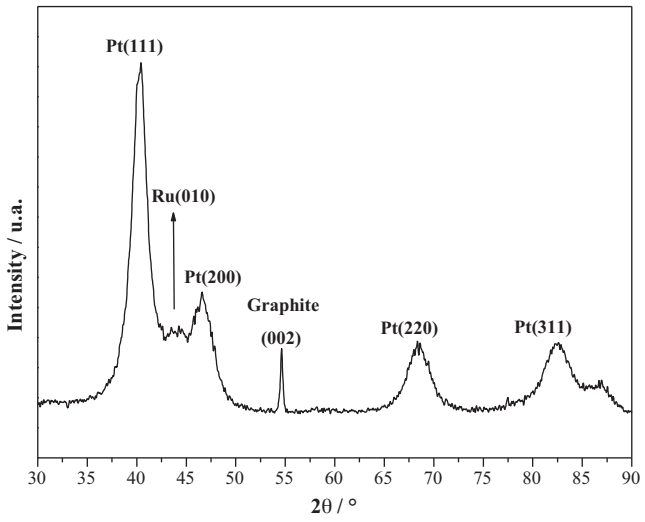

Fig. 9. X-ray pattern of 60 wt.% of PtRu(1:1) supported on MCC-SBA-15(1/3).

organized porosity on the silica phase of the MCCs facilitates the mass transport.

3.3. MCC-SBA-15(1/3) as anode for DMFC

The diffusion of the liquid combustible through the catalyst layer in the anode is more difficult than that of the gas oxidant in the cathode, thus a porous support as the MCC-SBA-15 could be an interesting alternative. The anode catalyst was prepared supporting 60 wt.% of platinum–ruthenium [5] (1/1 molar ratio) alloy on MCC-SBA-15(1/3) and Vulcan XC-72R. The catalyst alloy is composed by 39.26 wt.% of Pt, 21.74 wt.% of Ru and 40% of support.

The average size of the PtRu alloy crystallites on MCC-SBA-15(1/3) were determined as 3.6 nm by the Scherrer equation using the (2 2 0) diffraction peak (Fig. 9). The PtRu(1/1 molar ratio) alloy XRD pattern, shown in Fig. 9, reveals peaks assigned to (1 1 1), (2 0 0), (2 2 0), (3 1 1) and (2 2 2) planes, as observed for platinum XRD pattern, but slightly shifted to higher 2θ values, indicating a face-centered cubic symmetry with lower lattice parameters. This result is in accordance with the literature, where it is described that for PtRu alloy up to about 0.7 Ru atomic fractions, Pt and Ru form a solid solution with Ru atoms replacing Pt atoms on the lattice points of the face-centered cubic structure, leading to a decrease in the lattice parameters [28]. Above this value, Pt atoms replacing Ru in a hexagonal close packed structure [28]. Another peak at 44° 2θ is assigned to ruthenium (0 1 0) plane indicating the presence of non-alloyed ruthenium [29]. The peak of graphite (0 0 2) plane is also observed.

The PtRu alloy particles were also analyzed by TEM images (Fig. 10A) either in the raw state or upon occlusion in an epoxide resin and lamination. This last procedure aimed at verifying if alloy nanoparticles would be found inside the silica grains (Fig. 10B).

As shown in Fig. 10A, the PtRu particles (black dots) with dimensions between 2 and 5 nm were found inside the silica grains. In Fig. 10B, it was confirmed that the metal particles (black regions in the figure) are effectively supported inside the molecular sieve channels.

The 60 wt.% PtRu on MCC-SBA-15(1/3) was used as metal support for the DMFC anode and its performance was compared with that of the commercial support Vulcan XC-72R with the same metal loading, as shown in Fig. 11. Although for the studied of MCCs as DMFC cathode 20 wt.% Pt catalysts were used, it was not observed significant differences between catalysts with 20 or 50 wt.% Pt loading (see supporting information, Fig. S4). Hence, for the following tests, the cathode was prepared with the commercial Pt(50 wt.%)/Vulcan XC-72R (E-TEK). The cathode and the anode were fed, respectively, with 300 mL min^{-1} of non-humidified air and the 1 mL min^{-1} of a 1 mol L^{-1} aqueous methanol solution; the measurements were carried out at temperatures between 30 and 90 °C. The results are shown in Fig. 11.

For both samples tested as anode for DMFC it is observed a clear increase in the cell performance when the temperature is increased up to 90 °C due to higher reaction rates and improvement of the mass transport.

The results of current density at 0.2 V and maximum power density showed that the MCC-SBA-15(1/3) presented performance 5 and 10% lower than the commercial support Vulcan XC-72R at 30 and 40 °C, respectively. At 50, 60, 70, 80 and 90 °C, it presents performances 10, 12, 21, 6 and 17% higher. This behavior of increasing the MCC-SBA-15(1/3) performance as a function of the temperature, reaching an optimum point at 70 °C was also observed when the support was used on the cathode, as discussed before.

It is interesting that when used as cathode the MCC-SBA-15(1/3) cannot reach performances comparable to the Vulcan XC-72R, while the performances are comparable, or even better, when it is used as anodes. This is probably because the liquid combustible can diffuse better in the organized porous MCCs structure than in the Vulcan XC-72R structure, thus, reaching the catalytic sites without difficulty.

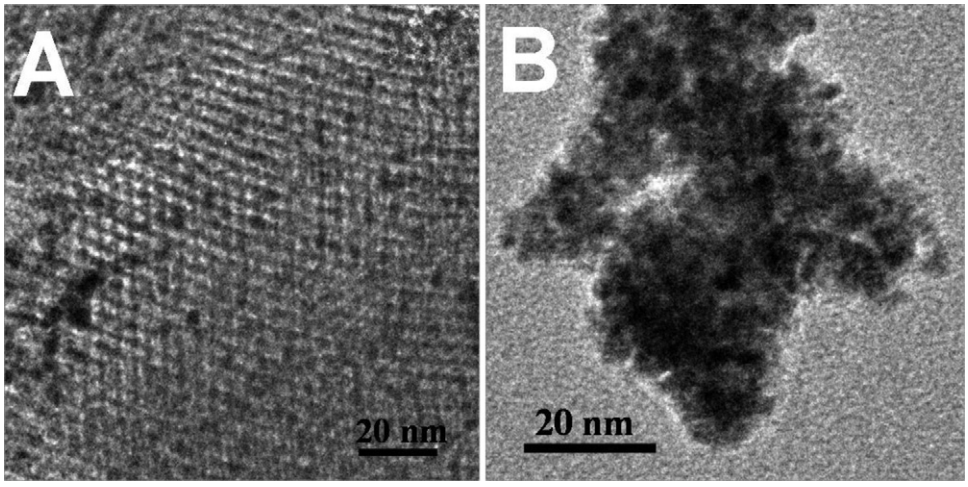

Fig. 10. TEM images of PtRu/MCC-SBA-15.

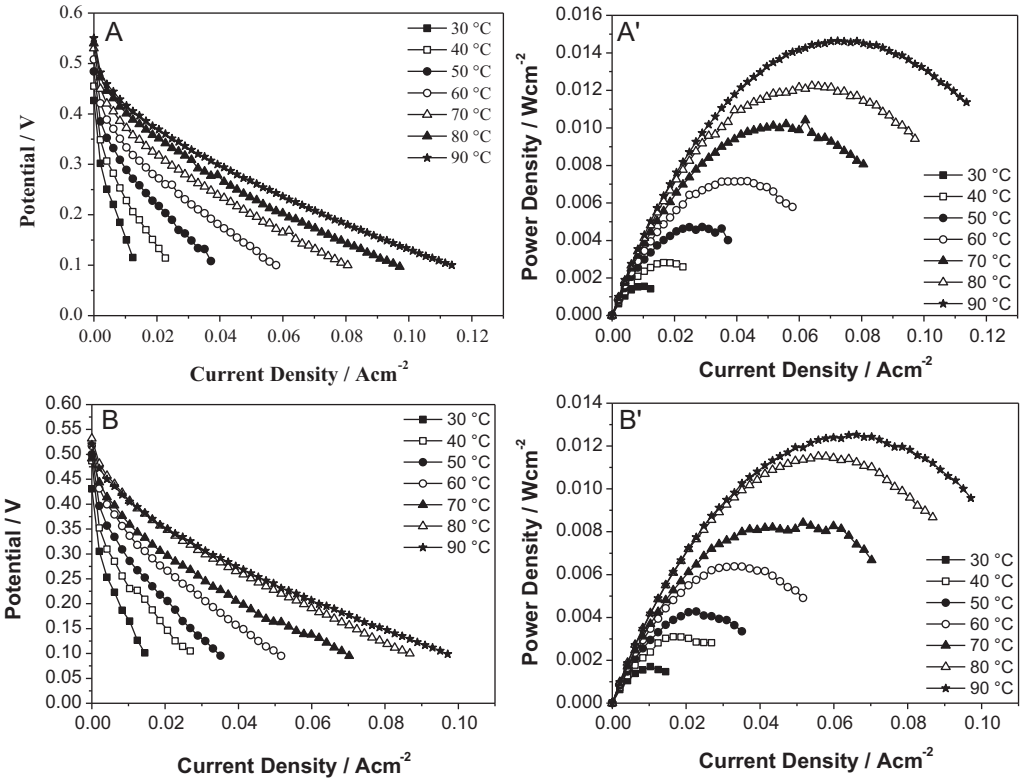

Fig. 11. Polarization and power curves obtained at different temperatures for the DMFC assembled with (A, A′) PtRu(60 wt.%) MCC-SBA-15(1/3), (B, B′) PtRu(60 wt.%) Vulcan XC-72R as metal support on the DMFC anode. Cathode was prepared using the commercial Pt(50 wt.%)/Vulcan XC-72R (E-TEK). Cathode and anode were fed, respectively, with 300 mL min^{-1} of air and 1 mL min^{-1} of a 1 mol L^{-1} aqueous methanol solution.

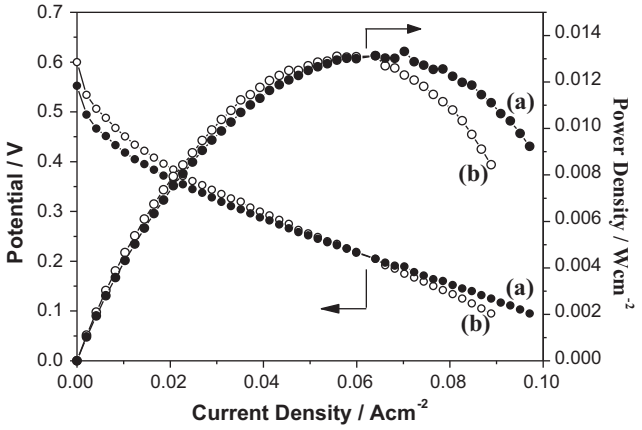

Fig. 12. Polarization (left hand side *y* axis) and power (right hand side *y* axis) curves obtained at 70 °C feeding the cathode with 100 mL min^{-1} of oxygen. The DMFC was assembled with (a) PtRu/MCC-SBA-15(1/3) and (b) PtRu/Vulcan XC-72R. Cathode was prepared using the commercial Pt(50 wt.%)/Vulcan XC-72R (E-TEK). The anode was fed with 1 mL min^{-1} of a 1 mol L^{-1} aqueous methanol solution.

These results are in accordance to those obtained by Yu et al. [30]. They found that the silica-templated mesoporous carbon when used on anode for DMFC carbon presents 16% higher performance than the Vulcan XC-72R.

Alternatively, the experiment was carried out at 70 °C, feeding the cathode with 100 mL min^{-1} of non-humidified oxygen instead of 300 mL min^{-1} of air and the anode with a 1 mL min^{-1} of a 1 mol L^{-1} aqueous methanol solution. The results are shown in Fig. 12.

When oxygen fed the cathode, the systems using MCC-SBA-15 (Fig. 12a) or Vulcan XC-72R (Fig. 12b) in the anode presented similar performances reaching 64.5 mA cm^{-1} of current density at 0.2 V and 13.1 mW cm^{-1} of maximum power density. The use of the pure oxidant implies in an increase of the reaction rate on the cathode and minimizes the anode effect.

4. Conclusions

A new family of MCC composites for electrodes designed to take the advantages of the well ordered mesoporous silica structure and of the graphite high conductivity, is here presented for the first time. X-ray diffraction confirmed the ordered structure of the composites, and nitrogen adsorption at −196 °C showed a decrease of the pore volume and surface area of MCC composites in comparison to the pure silica materials. Pore diameter of the silica counterpart in the composite was not affected by the graphite addition. SEM images revealed that in the composites with SBA-15 particle morphology is similar to a mechanical mixture.

The MCC-SBA-15 with SiO_2/C weight ratio of 1/3 was active on the DMFC cathode. However, the performance was significantly lower than that obtained with Vulcan XC-72R. Otherwise, when used as anode, the MCC-SBA-15 with SiO_2/C weight ratio of 1/3 showed performance comparable to (or somehow better than) the system using Vulcan XC-72R. This behavior can be explained by the more difficult diffusion of the liquid combustible if compared with the gas oxidant. The fuel can diffuse better in the organized porous MCC structure than in the Vulcan XC-72R structure while for the diffusion of the oxidant the structure studied did not show to be determinant.

Acknowledgments

The authors acknowledge the Piedmont Region (Microcell Project) and the "Fundação de Amparo à Pesquisa no Estado de São

Paulo", FAPESP, for the financial support to this work. JMRG thanks Ministero dell'Istruzione, dell'Università e della Ricerca for the PhD fellowship.

Appendix A. Supplementary data

Supplementary data associated with this article can be found, in the online version, at doi:10.1016/j.jpowsour.2011.05.008.

References

[1] 2007 Worldwide Fuel Cell Industry Survey, US Fuel Cell Council, pp. 1–8, http://www.usfcc.com/resources/2007worldwide_survey_final_low.pdf [last access 05 December 2010].
[2] 2008 Energy Technology Perspectives, Scenarios & Strategies to 2050, International Energy Agency, 2008, OECD Publishing, Paris, France, ebook version, p. 267.
[3] S. Litster, G. McLean, J. Power Sources 130 (2004) 61.
[4] X. Yu, S. Ye, J. Power Sources 172 (2007) 133.
[5] H. Liu, C. Song, L. Zhang, J. Zhang, H. Wang, D.P Wilkinson, J. Power Sources 155 (2006) 95.
[6] T. Matsumoto, T. Komatsu, K. Arai, T. Yamazaki, M. Kijima, H. Shimizu, Y. Takasawa, J. Nakamura, Chem. Commun. (2004) 840;
H. Tang, J.H. Chen, Z.P. Huang, D.Z. Wang, Z.F. Ren, L.H. Nie, Y.F. Kuang, S.Z. Yao, Carbon 42 (2004) 191.
[7] W. Li, C. Liang, J. Qiu, W. Zhou, H. Han, Z. Wei, G. Sun, Q. Xin, Carbon 40 (2002) 791;
W. Li, C. Liang, J. Qiu, W. Zhou, A. Zhou, Z. Wei, G. Sun, Q. Xin, J. Phys. Chem. B 107 (2003) 6292;
W. Li, C. Liang, W. Zhou, J. Qiu, H. Li, G. Sun, Q. Xin, Carbon 42 (2004) 436.
[8] G. Che, B.B. Lakshmi, C.R. Martin, E.R. Fisher, Langmuir 15 (1999) 750.
[9] G. Girishkumar, K. Vinodgopal, P. Kamat, J. Phys. Chem. B 108 (2004) 19960.
[10] J.S. Yu, S. Kang, S.B. Yoon, G. Chai, J. Am. Chem. Soc. 124 (2002) 9382;
G.S. Chai, S.B. Yoon, J.S. Yu, J.H. Choi, Y.E. Sung, J. Phys. Chem. B 108 (2004) 7074.
[11] G.S. Chai, S.B. Yoon, J.H. Kim, J.S. Yu, Chem. Commun. (2004) 2766.
[12] Y.C. Liu, X.P. Qiu, Y.Q. Huang, W.T. Zhu, J. Power Sources 111 (2002) 160;
Y.C. Liu, X.P. Qiu, Y.Q. Huang, W.T. Zhu, Carbon 40 (2002) 2375.
[13] M. Tsionsky, G. Gun, V. Giezer, O. Lev, Anal. Chem. 66 (1994) 1747.
[14] L. Rabinovich, O. Lev, Electroanalysis 13 (2001) 265.
[15] D. Zhao, Q. Huo, J. Feng, B.F. Chmelka, G.D. Stucky, J. Am. Chem. Soc. 120 (1998) 6024.
[16] S.H. Joo, S.J. Choi, I. Oh, J. Kwak, Z. Liu, O. Terasaki, R. Ryoo, Nature 412 (2001) 169.
[17] T.C. Deivaraj, J.Y. Lee, J. Power Sources 142 (2005) 43.
[18] J.M.R. Gallo, U.A. Icardi, V. Baglio, A. Coralli, A. Graizzaro, Int. J. Hydrogen Energy, doi:10.1016/j.ijhydene.2011.01.051.
[19] J. Gun, M. Tsionsky, L. Rabinovich, Y. Golan, I. Rubinstein, O. Lev, J. Electroanal. Chem. 395 (1995) 57.
[20] P. Alexandridis, U. Olsson, B. Lindman, Langmuir 14 (1998) 2627.
[21] A. Kukovecz, T. Kanyó, Z. Kónya, I. Kiricsi, Microporous Mesoporous Mater. 80 (2005) 85.
[22] S. Lowell, J.E. Shields, M.A. Thomas, M. Thommes, Characterization of porous solids and powders: surface area, pore size and density, Particle Technology Series, Springer, Dordrecht, NE, 2006, pp. 12–14, 37–46, 112–121.
[23] D.Y. Zhao, J.L. Feng, Q.S. Huo, N. Melosh, G.H. Fredrickson, B.F. Chmelka, G.D. Stucky, Science 279 (1998) 548.
[24] S. Manne, J.P. Cleveland, H.E. Gaub, G.D. Stucky, P.K. Hansma, Langmuir 10 (1994) 4409.
[25] X.W. Teng, H. Yang, J. Am. Chem. Soc. 125 (2003) 14559.
[26] W. Li, W.J. Zhou, H.Q. Li, Z.H. Zhou, B. Zhou, G.Q. Sun, X. Qin, Electrochim. Acta 49 (2004) 1045.
[27] E.P. Ambrosio, C. Francia, M. Manzoli, N. Penazzi, P. Spinelli, Int. J. Hydrogen Energy 33 (2008) 3142.
[28] E. Antolini, Mater. Chem. Phys. 78 (2003) 563–573.
[29] C. Roth, N. Martz, H. Fuess, Phys. Chem. Chem. Phys. 3 (2001) 315.
[30] J.-S. Yu, S. Kang, S.B. Yoon, G. Chai, J. Am. Chem. Soc. 124 (2002) 9382.